Reduction and precipitation of chromium(VI) using a palladized membrane biofilm reactor

Chengyang Wu, Jingzhou Zhou, Si Pang, Lin Yang, Eric Lichtfouse, Hongbo Liu, Siqing Xia, Bruce E Rittmann

Water Research 249 (2024) 120878

https://doi.org/10.1016/j.watres.2023.120878

Reduction and precipitation of chromium(VI) using a palladized membrane biofilm reactor

Chengyang Wu [a,1], Jingzhou Zhou [b,1], Si Pang [b], Lin Yang [b], Eric Lichtfouse [c], Hongbo Liu [a,*], Siqing Xia [b], Bruce E. Rittmann [d]

[a] School of Environment and Architecture, University of Shanghai for Science and Technology, 516 Jungong Road, Shanghai, China
[b] State Key Laboratory of Pollution Control and Resource Reuse, College of Environmental Science and Engineering, Tongji University, 1239 Siping Road, Shanghai, China
[c] Aix-Marseille Univ, CNRS, IRD, INRA, Coll France, CEREGE, Aix-en-Provence 13100, France
[d] Biodesign Swette Center for Environmental Biotechnology, Arizona State University, 727 Tyler Road, Tempe, USA

ARTICLE INFO

Keywords:
Membrane biofilm reactor
Palladium nanoparticle
Biofilm
Chromate reduction
Total Cr removal

ABSTRACT

H_2-driven reduction of hexavalent chromium (Cr(VI)) using precious-metal catalysts is promising, but its implementation in water treatment has been restricted by poor H_2-transfer efficiency and high catalyst loss. We investigated the reduction of Cr(VI) through hydrogenation catalyzed by elemental-palladium nanoparticles (PdNPs) generated *in-situ* within biofilm of a membrane biofilm reactor (MBfR), creating a Pd-MBfR. Experiments were conducted using a Pd-MBfR and a non-Pd MBfR. The Pd-MBfR achieved Cr(VI) (1000 μg L^{-1}) reduction of >99 % and reduced the concentration of total Cr to below 50 μg L^{-1}, much lower than the total Cr concentration in the non-Pd MBfR effluent (290 μg L^{-1}). The Pd-MBfR also had a lower concentration of dissolved organic compounds compared to the non-Pd MBfR, which minimized the formation of soluble organo-Cr(III) complexes and promoted precipitation of $Cr(OH)_3$. Solid-state characterizations documented deposition of $Cr(OH)_3$ as the product of Cr(VI) reduction in the Pd-MBfR. Metagenomic analyses revealed that the addition and reduction of Cr (VI) had minimal impact on the microbial community (dominated by *Dechloromonas*) and functional genes in the biofilm of the Pd-MBfR, since the PdNP-catalyzed reduction process was rapid. This study documented efficient Cr(VI) reduction and precipitation of $Cr(OH)_3$ by the Pd-MBfR technology.

1. Introduction

Chromium (Cr) contamination in water stems from a variety of industries: e.g., petroleum refining, wood preservation, electroplating, and pigment manufacture (Jobby et al., 2018). Cr in water is a serious concern because of its damage to the cardiovascular system and digestive tract (Pradhan et al., 2017); the U.S. Environmental Protection Agency (EPA) set a maximum contaminant level (MCL) for total Cr in drinking water at 100 μg L^{-1} (U.S. EPA, 2015).

Cr normally exists in hexavalent (Cr(VI)) and trivalent (Cr(III)) forms in water (Pradhan et al., 2017). Because Cr(III) forms precipitates with hydroxides at neutral or alkaline pH and is less toxic than Cr(VI), reduction of Cr(VI) to Cr(III), followed by solid separation to remove Cr (III), is a feasible means for Cr removal from water. Microbial reductions of Cr(VI) to Cr(III) has aroused keen interests in past decades due to their economic and environmental advantages (Zhao et al., 2022). However, several technical challenges such as long start-up period, limited Cr(VI) loading, and inhibition by oxygen and/or nitrate in water still exist (Thatoi et al., 2014). Of special concern is that extracellular polymeric substances (EPS) and some dissolved organic metabolites excreted by microorganism can bind with the free Cr(III) ion and compete with Cr $(OH)_3$ precipitation (Dogan et al., 2011; Kantar et al., 2008). As a result, the total Cr concentrations in bioreactor effluents could reach 200–300 μg L^{-1} (Lai et al., 2016; Long et al., 2017).

Hydrogenation catalyzed by platinum-group metals (i.e., platinum, palladium, rhodium, ruthenium, and iridium) can reduce Cr(III) with fast kinetics that lead to more precipitation (Yin et al., 2018; Zhou et al., 2021). Among the metals, palladium (Pd) efficiently adsorbs hydrogen (H_2) and converts it to atomic hydrogen (H^*_{ads}) that is active to cleave the Cr=O bond in chromate and form H_2O and reduced Cr(III) (Celebi et al., 2016). Pd is commonly applied as nanoparticles supported on another solid material, such as aluminum oxide, silicon dioxide, and

* Corresponding author.
E-mail address: Liuhb@usst.edu.cn (H. Liu).
[1] These authors contributed equally to this work.

Table 1
Parameters for operations and average performance for each stage of the Pd-MBfR or the non-Pd MBfR experiments at steady state.

stage	days	HRT	TCr						NO_3^--N					
			In (mg L^{-1})	surface loading (g m^{-2} d^{-1})	out (mg L^{-1})		removal flux (g m^{-2} d^{-1})		In (mg L^{-1})	surface loading (g m^{-2} d^{-1})	out (mg L^{-1})		removal flux (g m^{-2} d^{-1})	
					Pd-MBfR	MBfR	Pd-MBfR	MBfR			Pd-MBfR	MBfR	Pd-MBfR	MBfR
Stage 1	0–15	2h	0	–	–	–	–	–	5	0.39	0	0	0.39	0.39
Stage 2	16–40		0.5	0.040	0.032	0.20	0.038	0.024						
Stage 3	40–70		1	0.080	0.042	0.28	0.077	0.057						

graphene (Celebi et al., 2016; Xi et al., 2022). These Pd-based catalysts have drawbacks: Pd is expensive, and the chemical synthesis of the nanocatalysts requires large chemical and energy inputs (Munoz et al., 2017) and also produces secondary pollutants (Guo et al., 2018). Furthermore, the low water solubility and combustibility of H_2 makes conventional gas-transfer methods impractical (Zhou et al., 2019).

The membrane biofilm reactor (MBfR) overcomes the problems of Pd-catalyzed hydrogenation by efficiently and safely delivering H_2 to a biofilm through bubble-free diffusion across the walls of hollow-fiber membranes. The MBfR allows for the recovery of Pd from mining waste streams containing soluble Pd(II) and generate Pd(0) nanoparticles (PdNPs) captured in biofilms, which significantly reduces the cost of generating nanocatalysts (Zhou et al., 2016). The MBfR generates well-dispersed PdNPs without the need for adding polymeric stabilizer ligands or nanoclusters. The PdNPs, which accumulate within the biofilm attached to the H_2-transfer membranes, enable the *in-situ* reduction of oxidized contaminants (Long et al., 2021; Wu et al., 2022a). An MBfR with PdNPs in its biofilm, termed a Pd-MBfR, operates at ambient conditions and provides an environmentally friendly approach for synthesizing Pd nanocatalysts and using them for the reduction and removal of Cr.

We developed a Pd-MBfR capable of continuously removing Cr(VI) and total Cr (TCr). An MBfR without PdNPs was operated in parallel as a control. The primary objective of this study was to investigate the performance of Cr(VI) reduction and Cr recovery in the Pd-MBfR. An allied objective was documenting the fate of Cr through an analysis of the Cr (VI)-reduction products and their distribution within biofilm. The third objective was to elucidate how the microbial community within the biofilms adapted to Cr(VI) stress and determine the impact of bacterial metabolites on the solubility of total Cr in the effluents. On the one hand, Cr(VI) induces cell lysis and the secretion of organic compounds that may bind with the reduced Cr(III), leading to a high concentration of total Cr in the effluent (Dogan et al., 2011; Luo et al., 2022). On the other hand, organic compounds derived from the biofilm possess functional groups, such as the carboxylic groups (COOH), that can be ligands for binding Cr(III) ions (Cettn et al., 2009).

2. Materials and methods

2.1. Reactor figuration and setup

Experiments were conducted in parallel using two reactors similar to previous work and illustrated in Fig. S1 in Supporting Information (Wu et al., 2021). Briefly, each reactor had dual glass tubes connected by Viton tubing (Saint-Gobain, USA). One tube containing a bundle of 50 nonporous polypropylene hollow-fiber membranes (Teijin, Japan) with both ends connected to the H_2 gas pipeline, and the other tube contained a coupon bundle of 10 identical fibers with top end connected to the H_2 pipeline. The reactor had a working volume of 65 mL with a total membrane surface area of 95 cm^2. One peristaltic pump (Longer, China) introduced the influent medium to the MBfR, and another recirculation pump mixed the liquid of the reactor completely. The temperature was maintained at 25 ± 2 °C.

2.2. Inoculation, feeding, and startup of the MBfRs

In each MBfR, we introduced 10 mL of anoxic sludge obtained from the Wusong wastewater treatment plant (Shanghai, China) and allowed a biofilm to form by recirculating a mineral salt medium containing 14 mg L^{-1} NO_3^--N for 48 h. After the batch period, the reactors were continuously fed with a medium containing 10 mg L^{-1} NO_3^--N to accumulate biofilms on the membranes. The composition of the basic medium is summarized in supplementary Table S1. The H_2 pressure was maintained at 15 psig (2.0 atm absolute pressure). After two months, mature biofilms had formed in the MBfRs.

2.3. Synthesis of PdNP to create the Pd-MBfR

We introduced Pd(II) medium (160 mg L^{-1} Pd(II) as Na_2PdCl_4) into one MBfR in batch mode with the H_2 pressure of 15 psig (2.0 atm) to produce PdNPs within the biofilm (Pd-biofilm). The composition of the Pd(II)-containing medium was provided in a previous study (Wu et al., 2022b). The Pd(0)-deposition process lasted 48 h until a dark Pd-biofilm formed on the fibers and more than 99 % of the input Pd(II) was recovered after each addition. The created Pd-MBfR retained 11 mg total Pd.

2.4. Continuous operation for Cr(VI) removal

Continuous operation in the Pd-MBfR and the non-Pd MBfR was divided into three stages, each of which had an influent flow rate of 0.53 mL·min^{-1}, H_2 pressure of 15 psig, and a denitrification feed medium having 5 mg L^{-1} NO_3^--N. The influent medium was degassed with N_2 for 15 min prior to use, and this led to a dissolved oxygen (DO) concentration in the influent medium < 0.15 mg·L^{-1}. The pH of the influent was 7.1 ± 0.2.

After the biofilms fed with NO_3^- were stabilized at the end of Stage 1 (Day 1–15), we fed the reactors with the basic medium containing 5 mg L^{-1} NO_3^--N plus 0.5 mg L^{-1} Cr(VI) in Stage 2 (Day 16–40) and increased it to 1.0 mg L^{-1} in Stage 3 (Day 41–70). Operating conditions in all stages are summarized in Table 1. We operated each stage until it reached the steady-state, which occurred when the effluent concentrations of Cr(VI) and NO_3^- were stable (< 10 % variation) for at least consecutive 3 days.

2.5. Analytical methods

The liquid samples in the MBfRs were collected using 5-mL syringes and filtered through 0.22-μm PVDF membrane filters. The Cr(VI) concentration was analyzed by a diphenyl carbazide method (Method 3500-Cr D, APHA, 1998). The concentrations of Pd(II) and Cr (Cr(III)+Cr(VI)) were assayed by inductively coupled plasma-mass spectrometry (ICP-

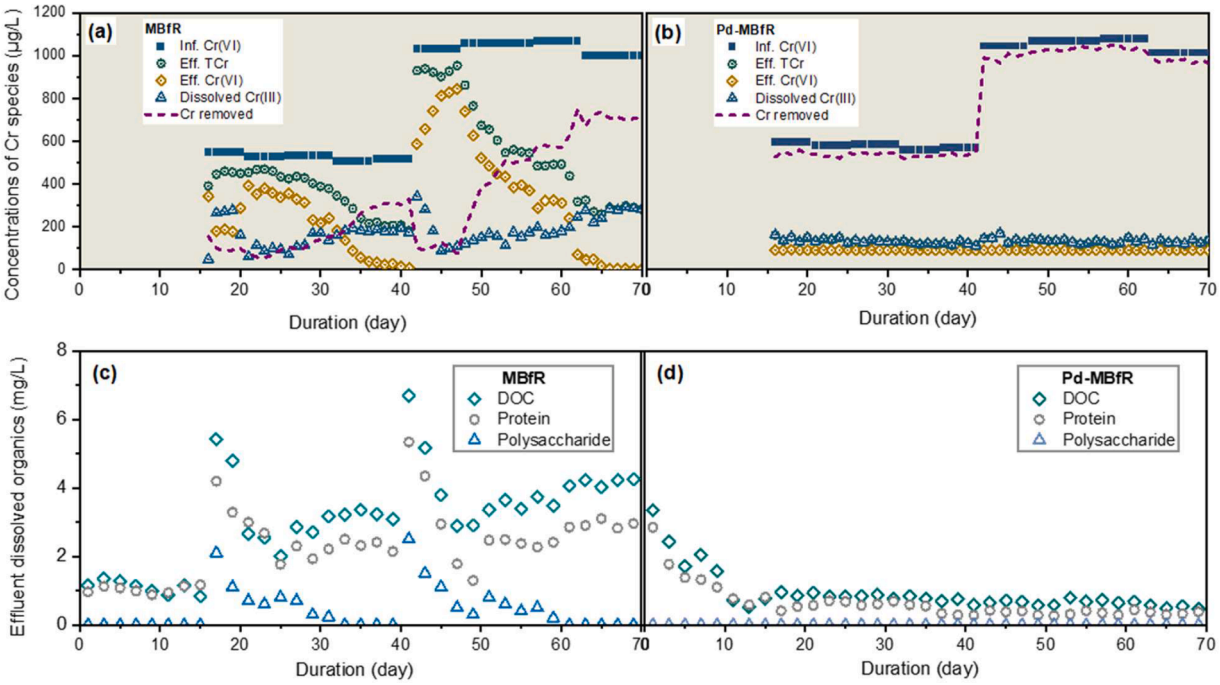

Fig. 1. Concentrations of influent Cr(VI), effluent total Cr and effluent dissolved Cr(III), and Cr removed in the non-Pd MBfR (a) and the Pd-MBfR (b); concentrations of effluent DOC, protein, and polysaccharide in the non-Pd MBfR (c) and the Pd-MBfR (d).

MS, Agilent Technologies7700, USA). Unfiltered samples were also collected and digested using thick hot mixture of hydrochloric acid and nitric acid to dissolve any solid Pd. Both the filtered and unfiltered samples were assayed for the concentrations of soluble and total Pd, respectively. Dissolved organic carbon (DOC) was measured using a total organic carbon analyzer (TOC, Shimadzu TOC-L, Japan). NO_3^- and NO_2^- were analyzed by an ion chromatograph (IC, Dionex Aquion, USA) with an AS-19 column. pH and DO were measured using a multi-Parameter Meter (HACH HQ40d, USA).

The fluorescence spectra of the liquid samples were analyzed using an excitation-emission matrix (EEM) fluorescence spectrophotometer (Hitachi, F-700, Japan), and deionized water was used as the blank. Table S2 provides detailed information of the five fluorescence regions in the fluorescence spectrum, and the specific parameter settings for these instruments can be found in Table S3. The concentrations of protein and carbohydrate were analyzed, respectively, by a Coomassie brilliant blue G-250 method (Pierce and Suelter, 1977) using bovine serum albumin (Sigma, USA) as the standard, the phenol-sulfuric acid method (Frølund et al., 1996) using glucose as the standard.

2.6. Solid-state characterization

We collected solid samples from the two reactors at end of Stages 1 and 3 by cutting off ~5-cm-long fiber pieces from the coupon bundles. After chemical fixation and ultra-microtome slicing, these fibers were characterized using transmission electron microscopy (FEI Tecnai G2 F20, USA) coupled with energy-dispersive X-ray spectroscopy (EDX). In addition, we scratched solids off the fibers and then immediately freeze-dried them for subsequent X-ray photoelectron spectrum (XPS; Thermo ESCALAB 250, USA), X-ray diffraction (XRD, Bruker D8 advance, Germany), and Fourier transform infrared spectroscopy (FTIR, Thermo TENSOR 37, USA) analyses. Detailed procedures of sample fixation/slicing and information on the instruments are in published works (Wu et al., 2022a, 2022b).

2.7. Microbial community analyses

At the end of Stages 1 and 3, we cut off a 10-cm section from a coupon fiber in each reactor. We followed the procedures of biofilm separation and DNA extraction described by Xia et al. (2016). After amplification and purification, the DNA was sent to Majorbio Technology (Shanghai, China) for Illumina MiSeq sequencing of the 16S rDNA gene with standard protocols. We processed the raw data using QIIME 1.9.1 suite (Caporaso et al., 2010), and the 16S rDNA data obtained from sequencing were further analyzed using Phylogenetic Investigation of Communities by Reconstruction of Unobserved States (PICRUSt) pipeline to predict the metagenomic compositions of the biofilms communities based on the latest Kyoto Encyclopedia of Genes and Genomes (KEGG) database (Langille et al., 2013; Xie et al., 2011). The detailed protocol and data analysis are listed in Supporting Information (SI).

To define if a certain functional gene was enriched in each biofilm compared to the denitrifying biofilm, we calculated the odds ratios as

$$\mathrm{OR} = \frac{\varphi_i/(1-\varphi_i)}{\varphi_1/(1-\varphi_1)} \quad (1)$$

where φ_i is the relative abundance of a specific metabolic category to given genes in the Pd-biofilm (Stage 1 or 3) or biofilm metagenomes (Stage 3), and φ_1 is the relative abundance of a specific metabolic category to given genes in the denitrifying biofilm metagenomes (Stage 1).

2.8. Flux calculations

The flux of a substrate (J) was calculated by

$$J = \frac{Q(C_i - C_e)}{A} \quad (2)$$

where J is the flux, g m^{-2} d^{-1}; Q is the influent flow rate, m^3 d^{-1}; C_i and C_e are influent and effluent concentrations of each substrate (Cr and NO_3^--N), g m^{-3}; and A is the effective membrane surface area, m^2.

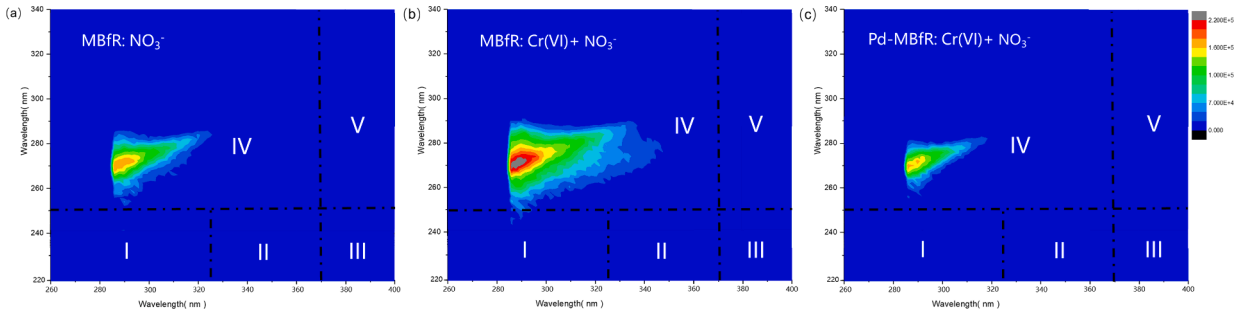

Fig. 2. The fluorescence signals for the effluent of MBfR exposed to NO_3^- (a), to NO_3^- and Cr(VI) (b); and the effluent of Pd-MBfR exposed to NO_3^- and Cr(VI) (c) analyzed by fluorescence spectrophotometer.

3. Results and discussion

3.1. Continuous tests of Cr(VI) reduction

3.1.1. Prompt and complete Cr removal in the Pd-MBfR

Continuous Cr(VI)-reduction experiments were conducted to investigate performances of the Pd-MBfR and in the MBfR without PdNPs. Table 1 summarizes conditions in all three stages. The effluent NO_3^--N and NO_2^--N concentrations are shown in Fig. S2. H_2 was not a rate-limiting factor, since the actual H_2 fluxes (~150 e^--meq m^{-2} d^{-1}) were much lower than the maximum theoretical H_2 flux (Tang et al., 2012) (420 e^--meq m^{-2} d^{-1}) in each stage. Each stage lasted from 15 to 30 days, providing sufficient time to reach a steady state for all chemical species.

After the biofilm in the non-Pd MBfR was stable at the end of Stage 1, the influent was set to a Cr(VI) concentration of 500 μg L^{-1} in Stage 2 (from day 16 to day 40). The effluent Cr(VI) concentration in the non-Pd MBfR slowly decreased to below 50 μg L^{-1} by the end of Stage 2 (Fig. 1a). During Stage 3, the influent Cr(VI) concentration was set to 1000 μg L^{-1}, with an influent loading of 80 mg Cr m^{-2}·d^{-1}. The Cr(VI) concentration in the non-Pd MBfR effluent increased from 8.7 μg L^{-1} to 800 μg L^{-1} within 4 days, and then it gradually decreased, reaching 10 μg L^{-1} after day 65. At this point, the TCr concentration was approximately 290 μg L^{-1}, achieving a Cr(VI) reduction ratio of 99 %, while the TCr removal ratio was ~70 %. In comparison, Cr(VI) in the effluent of the Pd-MBfR remained undetectable (detection limit of 0.05 μg L^{-1}) for Stages 2 and 3, and the TCr concentration at the end of Stage 3 was approximately 43 μg L^{-1}, with a TCr-removal efficiency up to 96 %.

We calculated the concentrations of removed Cr in both reactors as the difference between the concentration of influent Cr(VI) and effluent TCr (Fig. 1a and 1b). In the Pd-MBfR, more than 950 μg L^{-1} of Cr(III) was removed from the water through reduction and precipitation. In contrast, removed Cr in the non-Pd MBfR was about 700 μg L^{-1}. Thus, Pd-MBfR was superior over the non-Pd MBfR for reducing Cr(VI) and removing TCr. Furthermore, the Pd-MBfR needed no prolonged acclimation period, but promptly reduced Cr(VI) in the influent.

The simple conditional solubility of Cr(III) is 40–90 μg L^{-1} at pH 7.4–7.7 (Fig. S3). Hence, the presence of oversaturated Cr(III) from Cr (VI) reduction should lead to the formation of insoluble chromium hydroxide ($Cr(OH)_3$), which is crucial for efficient TCr removal. The dissolved Cr(III) concentration of 40–50 μg L^{-1} in the Pd-MBfR effluent was consistent with precipitation of $Cr(OH)_3$ down to near its conditional solubility. In contrast, the non-Pd MBfR's effluent contained higher dissolved Cr(III) (280–300 μg L^{-1}), which exceeded the conditional solubility of Cr(III) in neutral-pH water. The presence of a higher dissolved-Cr(III) concentration implies that much of the Cr(III) produced by reduction of Cr(VI) was complexed and not available to precipitate with the hydroxide anion. The likely complexing ligands were organic carboxylates, a topic discussed in Section 3.2.2.

3.1.2. PdNPs protect biofilm from Cr(VI) toxicity

The DOC in the bioreactor effluent originated from microbial activity, since the influent had no organic compounds. Before the addition of Cr(VI) to the influent, the effluent DOC concentration was ~0.9 mg L^{-1} in Stage 1 for both MBfRs. For the non-Pd MBfR, the DOC increased to ~3.0 mg L^{-1} in Stage 2 and 4.2 mg L^{-1} in Stage 3. This increase demonstrates Cr(VI) stress on the biofilm, as the bacteria responded by releasing organic matter, such as soluble Cr(VI) reductases, into the medium as a detoxification mechanism (Joutey et al., 2015). Furthermore, the introduction of Cr(VI) to the non-Pd MBfR led to sudden DOC peaks during the initial days of Stages 2 and 3. These sudden peaks in DOC concentration imply that the toxic effects of Cr(VI) brought also about cell lysis that released a large amount of soluble organic matter. By comparison, the DOC concentration in the effluent of Pd-MBfR remained stable at approximately 0.5 mg L^{-1}, indicating that PdNPs prevented Cr(VI) toxicity to biofilm.

3.1.3. The formation of organo-Cr(III) complexes increased Cr(III) solubility

Fig. 1a and 1c illustrate a positive relationship between a higher concentrations of DOC and the presence of proteins in the effluent for the higher effluent concentrations of Cr(III) in the non-Pd MBfR. The correlation among DOC, protein, and soluble Cr(III) support that the organic matter released by the biofilm enhanced the solubility of Cr(III) by complexing with Cr(III). Previous studies documented the formation of organo-Cr(III) complexes following enzymatic reduction of Cr(VI), with Cr(III) bonding to microbially produced ascorbate and glutathione (Thatoi et al., 2014). In addition, certain bacterial small-molecule metabolites (e.g., galacturonic, glucuronic, and alginic acids) can form soluble organo-Cr(III) complexes, thereby increasing Cr(III) conditional solubility (Dogan et al., 2011; Puzon et al., 2005).

For the fluorescence spectra in Fig. 2, region IV represents microbial products and protein-like substances (Table S2). The stronger fluorescence signal of the non-Pd MBfR's effluent compared to that of the Pd-MBfR confirms the higher concentrations of DOC and protein-like substances that accumulated in the non-Pd MBfR's effluent after the addition of Cr(VI). These findings support the idea that organic matter released by bacteria enhanced the solubility of Cr(III), providing an explanation for the Cr(III) concentrations that far exceeded the concentrations observed in the non-Pd MBfR's effluent.

3.1.4. Stability of Pd-biofilm during continuous operation

Intermittent monitoring of effluent Pd throughout Stages 2 and 3 (Fig. S4) revealed that the loss of solid Pd(0) exceeded the factor caused by Pd(II) leaching. The minimal concentration of soluble Pd(II) in effluent (0.47 ± 0.16 μg L^{-1}) at the end of Stage 3 suggests that efficient H_2-transfer to the PdNPs prevented oxidation to Pd(II) over the long-term. Detachment emerged as the primary cause to Pd(0) loss.

The cumulative loss of total Pd during the 55-day operation (660 HRTs) was 0.34 mg, or only 3.1 % of the total deposited Pd(0). Concurrently, a total of 32.42 mg of Cr(VI) was removed during this

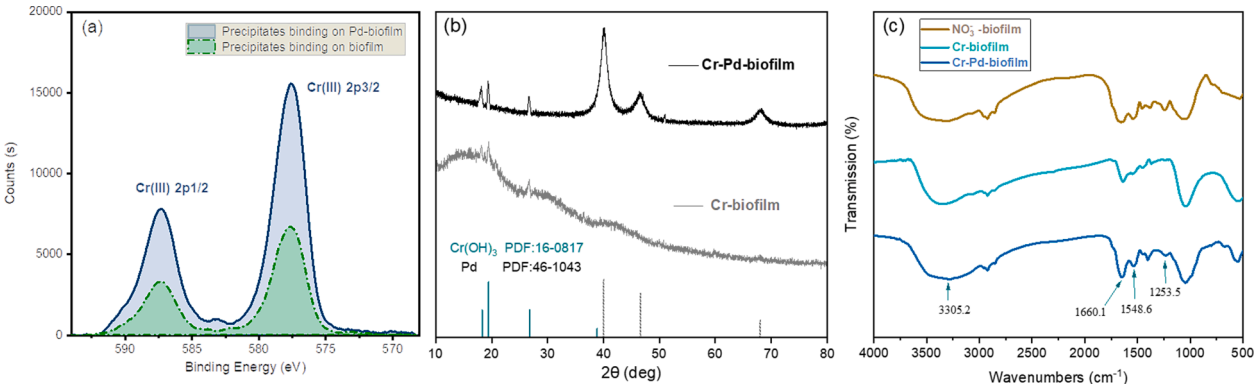

Fig. 3. XPS (a), XRD (b), and FTIR (c) analyses of the chromium precipitates binding on Pd-biofilm and biofilm, respectively.

period. Thus, the estimate of the mass ratio of Cr removal to Pd consumption would reach 100, even without considering the recovery of lost Pd(0) solid.

3.2. The fate of Cr

3.2.1. Cr reduction and in situ precipitation of $Cr(OH)_3$ on PdNPs

In the Pd-MBfR, the majority of produced Cr(III) was removed through precipitation (Fig. 1b), leading to a low concentration of TCr in the effluent. Furthermore, the TCr concentration with or without filtration was comparable (Fig. 1), which means that $Cr(OH)_3$ precipitates were deposited in the Pd-biofilm and retained in the Pd-MBfR. To evaluate the fate of Cr in the biofilm, Pd-biofilm samples were collected at the end of the experiment and analyzed using TEM-EDX, XPS, XRD, and FITR.

Fig. S5a presents the cross-sectional TEM image of the Pd-biofilm collected at the end of Stage 3. The results of EDX mapping, depicted in the Fig. S5a, indicate that the majority of reduced Cr(III) (confirmed by XPS data) was deposited on PdNPs, since the PdNPs were the primary sites for the reduction of Cr(VI). A minor amount of Cr precipitate was present in extracellular polymeric substances (EPS) and bacterial surfaces without PdNPs, indicating limited direct bioreduction of Cr(VI) within the Pd-MBfR system. The dominance of Pb-based reduction of Cr (VI) means that PdNPs, by accelerating the reduction of Cr(VI) and its precipitation/immobilization, effectively protected the bacteria from the toxic effects of Cr species.

Fig. 3a presents the XPS spectra of the solid samples from the biofilms. Peaks at 587 eV and 577 eV correspond to Cr(III) $2p_{1/2}$ and $2p_{3/2}$, respectively (Lai et al., 2016). The XPS spectrum provides further confirmation that a Cr(III) precipitate was the product of Cr(VI) reduction. Cr(III) was detected in samples from the Pd-MBfR and the non-Pd MBfR, but the XPS data also demonstrate that the concentration of Cr (III) in the Pd-biofilm was higher than that in biofilm, which is consistent with the effluent results observed during the continuous reduction experiments.

The XRD pattern (Fig. 3b) reveal the presence of $Cr(OH)_3{\cdot}3H_2O$ within the Pd-biofilm, with characteristic peaks observed at 2θ values of 18.2° (0 0 1), 19.4° (1 0 0), and 26.7° (1 0 1) (JCPDS No.16–0817). The Pd-biofilm had higher $Cr(OH)_3{\cdot}3H_2O$ content compared to the biofilm, while the concentration of Cr(III) in the non-Pd MBfR effluent (~290 μg L^{-1}) far exceeded the conditional solubility range of Cr(III) at pH 7.4–7.7 (i.e., 40–90 μg L^{-1}). Thus, most of the Cr(III) was precipitated as $Cr(OH)_3$ that deposited within the Pd-biofilm.

As the biofilm continues to grow, its adsorption capacity is supposed to steadily increases until it reaches its maximum when the biofilm becomes a "steady-state biofilm" (Rittmann and McCarty, 2020). At this stage, the biomass synthesis rate matches its loss rate. Metabolic degradation products generated by the biofilm processes, including decaying bacteria and EPS fragments, can detach from the biofilm under the influence of hydraulic shear, concurrently releasing the deposited Cr

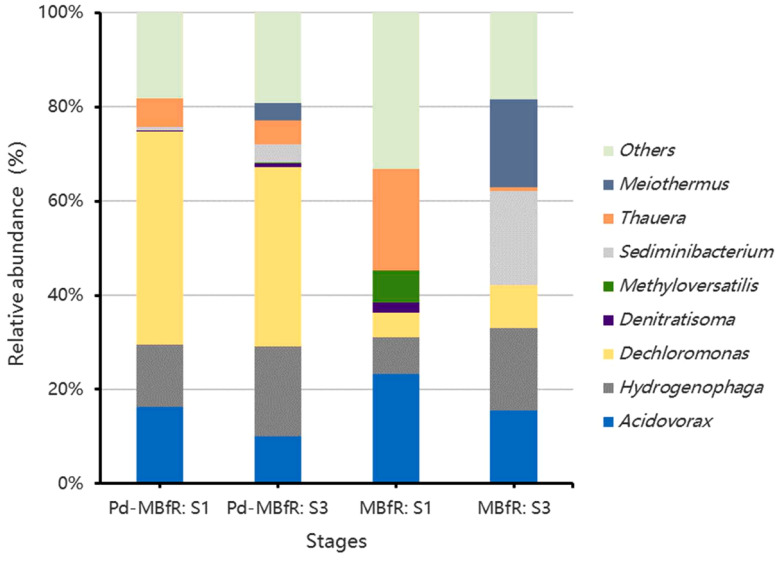

Fig. 4. Bacteria community structure of Pd-biofilm and biofilm at genus level. "Others" stands for the relative abundance summary of all genera with abundance less than 2 %.

Table 2
Relative abundance and odds ratios of predicted functional genes involved in metabolisms of Cr in Pd-biofilm and biofilms by PICRUSt analysis. Red highlight indicates an increase, while blue highlight indicates a decrease.

Functions	KEGG entry	Descriptions	Relative abundance ‰				OR			
			Pd-biofilm		biofilm		Pd-biofilm		biofilm	
			Stage 1	Stage 3	Stage 1	Stage 3	Stage 1	Stage 3	Stage 1	Stage 3
Hydrogen utilization	K00532 K00533 K00534 K06441	Ferredoxin hydrogenase, EC:1.12.7.2	2.5	2.0	4.2	4.7	0.61	0.49	1	1.13
	K18016 K18017	Membrane-bound hydrogenase subunit, EC:1.12.7.2	1.8	1.6	2.3	2.7	0.78	0.69	1	1.17
	K00437 K18008	[NiFe] hydrogenaselarge large subunit, EC:1.12.2.1	1.1	1.1	1.8	1.6	0.62	0.63	1	0.92
	K18005 K18006	[NiFe] hydrogenase diaphorase moiety large subunit, EC:1.12.1.2	9.0	8.5	17.2	15.9	0.53	0.49	1	0.93
	K05586 K05587 K05588	[NiFe] hydrogenase diaphorase subunit, EC:7.1.1.2	2.1	2.5	3.5	3.1	0.60	0.73	1	0.89
Nitrate reduction	K00360	Nitrate reductase (NADH), EC:1.7.99.-	5.6	5.9	4.7	4.2	1.19	1.26	1	0.90
	K00362	Nitrite reductase (NADPH) large subunit, EC:1.7.1.15	3.6	2.9	6.9	7.7	0.52	0.42	1	1.11
	K00363	Nitrite reductase (NADPH) small subunit, EC:1.7.1.15	2.5	2.1	3.7	3.1	0.68	0.57	1	0.85
	K00366 K00367	Ferredoxin-nitrite reductase, EC:1.7.7.1	0.4	0.3	0.6	0.5	0.59	0.46	1	0.75
	K00368	Nitrite reductase (NO-forming), EC:1.7.2.1	0.9	0.7	2.2	2.0	0.39	0.29	1	0.91
	K02305	Nitric oxide reductase, EC: 1.7.2.5	1.5	1.1	4.4	4.1	0.33	0.26	1	0.95
	K00376	Nitrous oxide reductase, EC:1.7.2.4	1.6	1.0	4.2	3.6	0.39	0.23	1	0.86
Chromate reduction	K19784	Chromate reductase, YieF	0.7	0.7	0.6	1.5	1.22	1.12	1	2.62
	K07240	Chromate transporter, ChrA	3.6	3.8	3.2	7.7	1.12	1.18	1	2.38
	K12262	Cytochrome b561	1.9	2.4	1.7	3.0	1.11	1.37	1	1.75
	K12263	Cytochrome c551	2.5	2.0	1.8	3.6	1.42	1.17	1	2.08
	K00383	Glutathione reductase (NADPH), EC:1.8.1.7	1.4	1.2	1.4	1.8	1.01	0.88	1	1.26
	K00384	Thioredoxin reductase (NADPH), EC:1.8.1.9	15.2	13.5	16.5	21.6	0.92	0.82	1	1.31
	K00344	Quinone reductase, EC:1.6.5.5	10.8	10.8	9.4	13.0	1.15	1.15	1	1.38
	K10678 K10679	Nitroreductase, EC:1.-.-.- 1.5.1.34	1.7	1.5	1.3	2.9	1.31	1.16	1	2.21
Organo-Cr(III) complexes formation	map00270	Cysteine metabolism	76.5	75.7	83.0	111.9	0.92	0.91	1	1.35
	map00480	Glutathione metabolism	46.5	45.5	51.3	76.0	0.91	0.89	1	1.49
	map00053	Ascorbate and aldarate metabolism	13.8	17.6	14.1	20.2	0.98	1.25	1	1.43
	map00620	Pyruvate metabolism	103.3	105.3	112.0	141.6	0.92	0.94	1	1.27
	map00340	Histidine metabolism	45.8	47.5	49.8	64.9	0.92	0.95	1	1.31
	map00260	Serine metabolism	76.3	72.2	71.0	72.1	1.08	1.02	1	1.02
Membrane transport	map03070	Bacterial secretion system	55.7	61.4	67.0	81.1	0.83	0.92	1	1.21
	map02010	ABC transporters	313.1	339.2	297.3	423.2	1.05	1.15	1	1.44
	map03060	Protein export	41.2	41.1	42.6	53.3	0.97	0.96	1	1.25

$(OH)_3$. The growing biofilm leads to an increased adsorption capacity, with the rate equal to the release rate of $Cr(OH)_3$ due to biomass loss. Consequently, the adsorption capacity of the $Cr(OH)_3$ precipitate within the biofilm should eventually reach a dynamic plateau.

3.2.2. Cr(III) complexed with the functional groups of biofilm after Cr bioreduction

Within the non-Pd biofilm, electron-dense precipitates were mostly intracellular or associated with the outer surface of the cells (Fig. S5b). Only a small fraction of precipitates was dispersed in EPS-like excretions attached to the cells. Exposure to Cr(VI) for the bacterial cells in the non-Pd MBfR's biofilms altered the cell shapes and caused acute damage, leading to cell lysis (indicated by the yellow arrow in the TEM image of Fig. S5b). The observed cell deformation can be attributed to the stress exerted by Cr on the cell membrane's efflux system, resulting from a substantial accumulation of Cr(III) within the cytoplasm (Ramírez-Díaz et al., 2008).

As shown in Fig. 3, the presence of Cr(III) in the non-Pd biofilm was verified by XPS spectra, and the absence of crystalline Cr(III) precipitates in XRD spectrum indicates that Cr(III) existed in an form of amorphous form as organo-Cr(III) complexes.

The spectra of the denitrifying biofilm exhibited distinct peaks at 3300 cm^{-1}, 1660 cm^{-1}, 1550 cm^{-1}, 1255 cm^{-1}, and 1180 cm^{-1}. The FTIR spectrum of the Pd-biofilm (Stage 3) was similar to that of the denitrifying biofilm. However, Cr(VI) reduction and its precipitation as $Cr(OH)_3$ in biofilm (Stage 3) led to a shift in the absorption peaks compared to the denitrifying biofilm. The Cr-reducing biofilm sample showed a broad, intense peak at around 3305 cm^{-1}, indicative of -OH stretching. The adsorption peaks at 1660 cm^{-1}, 1548 cm^{-1}, and 1253 cm^{-1} indicated the stretching vibration of C-O in carboxylic acid, the combination of γNH/γC=O in amide I, amide II, and O-H in carboxylic groups, respectively. These results are partly cross proved with Bahafid et al. (2011), who reported that Cr(VI) removal by *P. anomala* initially involved adsorption on functional groups (e.g., carboxyl group, amide I, amide II, amide III, polysaccharides, and sulfonate) of cell surfaces, followed by intracellular accumulation and reduction of Cr(VI) to Cr (III). FTIR results support the evidence of Cr(III)-forming complexes with biological ligands in the biofilm.

3.3. Characterization of the bacterial communities and their functional genes

3.3.1. Community structure

Fig. 4 shows that the predominant genus in the Pd-biofilm during NO_3^- reduction and Cr(VI) reduction (Stages 1 and 3) was *Dechloromonas*, which is commonly found in Pd(II)-reducing biofilms having similar pH conditions (Zhou et al., 2016). *Dechloromonas* is known for its versatile respiratory abilities, including for NO_3^- and metals such as U

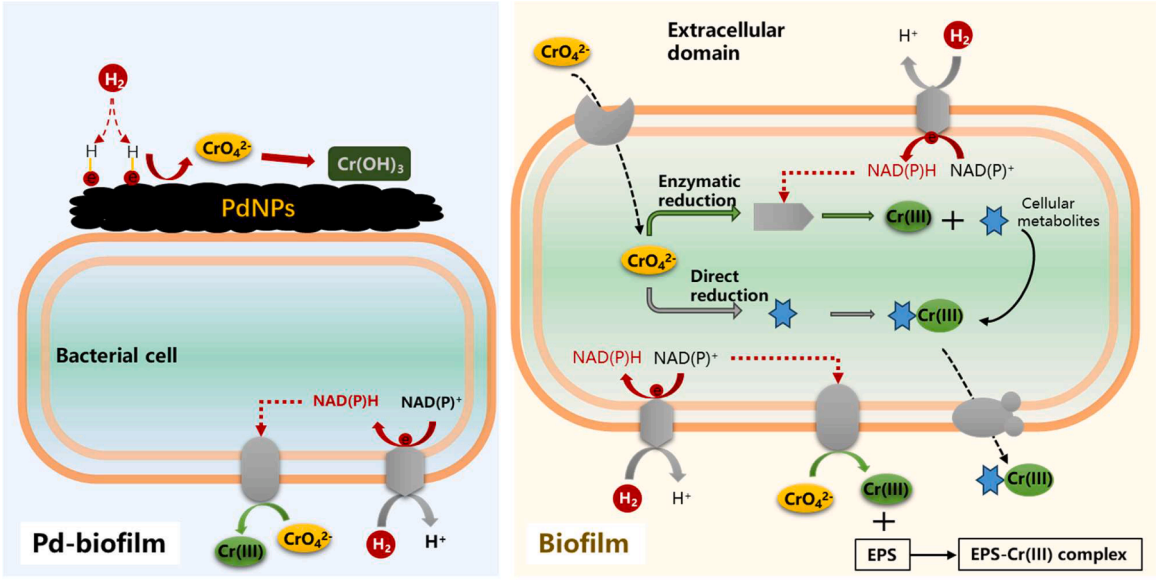

Fig. 5. Proposed pathways of Cr(VI) reduction and removal by a Pd-biofilm (left) or a non-Pd biofilm (right).

(VI) (Akob et al., 2008) and Fe(III) (Coby et al., 2011). Additionally, two autotrophic denitrifying genera, *Acidovorax* and *Hydrogenophaga*, remained stable in the Pd-biofilm before and after the addition of Cr(VI) (i.e., in Stages 1 and 3). Thus, the microbial community structure in the Pd-biofilm remained stable after Cr exposure, indicating minimal microbial stress from Cr(VI) toxicity in the Pd-biofilm, with denitrifiers and Pd-reducing bacteria maintaining dominance before and after Cr addition.

In the NO_3^--fed biofilm (non-Pd) during Stage 1, the dominant genera in the biofilm were denitrifiers (Fig. 4): *Acidovorax* (23 % of the overall community), *Thauera* (21 %), *Hydrogenophaga* (7.8 %), and *Dechloromonas* (5.2 %). For the non-Pd MBfR system, 55 days of exposure to Cr (VI) in Stages 2 and 3 shifted the dominant genus to *Sediminibacterium*, which constituted 20 % of the community, probably due to its metal resistance and Cr(VI)-reduction potential (Chi et al., 2023). *Meiothermus,* accounting for 19 % of the total bacteria, also was enriched in the biofilm, and it has demonstrated Cr(VI) reduction ability through a membrane-bound enzyme and a cytoplasmic enzyme in a CH_4-based MBfR (Lai et al., 2016). Thus, the introduction of Cr stimulated the growth of Cr-tolerant and reducing bacteria in the non-Pd biofilm, resulting in a shift from denitrifying bacteria to Cr-reducing bacteria.

3.3.2. *Functional genes*

We employed PICRUSt to predict the metagenomic functional-gene composition of the biofilms at all stages; the results are presented in Table 2. Since the overall community structure did not undergo significant changes upon the introduction of Cr(VI) in the Pd-MBfR, the corresponding variations in functional genes also were minimal. In Pd-biofilm, the relative abundance of genes predicted to be involved in H_2 utilization, nitrate reduction, formation of organo-Cr(III) complexes, and membrane transport proteins showed small changes from Stage 1 to Stage 3 (i.e., S1 and S3), although genes associated with chromate reduction were slightly more abundant in Pd-biofilm in S3. The predicted functional genes related to nitrite reduction were moderately suppressed by the presence of PdNPs due to the rapid reduction of nitrite by Pd catalysis (Long et al., 2021). Since PdNPs catalyzed the abiotic consumption of H_2 and competed with autotrophic bacteria for electron donors, genes encoding enzymes for hydrogen utilization were relatively less abundant in Pd-biofilm.

In the non-Pd biofilm, genes encoding chromate reductases (e.g., YieF, cytochrome b561, and cytochrome c551) significantly increased after addition of Cr(VI). YieF, a dimeric flavoprotein, intracellularly reduces chromate to Cr(III) using NADH as the reductant, while cytochrome b and c are membrane-bound reductases that reduce Cr(VI) by utilizing chromate as the terminal electron acceptor, resulting in Cr(III)-containing precipitates on the cell surface (Thatoi et al., 2014). The TEM analysis of the biofilm (Fig. S5b) reinforces these predicted pathways for chromate reduction. Furthermore, genes predicted to encode cellular organic metabolites involved in the generation of organo-Cr(III) complexes (e.g., cysteine, glutathione, ascorbate, pyruvate, and histidine) (Puzon et al., 2005) increased moderately. These compounds accelerate bioreduction of Cr(VI) and the formation of soluble Cr(III)-ligand complexes (Puzon et al., 2005). The increases in genes encoding Cr(VI) reduction, cellular organic metabolites, and membrane transport provide strong evidence that the presence of Cr(VI) induced bacterial resistance to Cr, leading to the release of proteinaceous extracellular secretions (Fig. 2). These secretions contribute to the detoxification of Cr and the formation of organo-Cr(III) complexes, which enhanced the solubility of Cr(III).

In summary, after exposure to Cr(VI), the Pd-biofilm did not experience a significant increase in the abundance of functional genes related to chromate reduction and cellular metabolites involved in the producing organo-Cr(III) complexes, but non-Pd biofilm showed major increases. The lack of Cr resistance metabolisms in the Pd-biofilm support that the PdNPs protected the microorganisms from the toxic effects of Cr, which prevented the formation of soluble organo-Cr(III) and enhanced TCr removal efficiency.

3.4. *Proposed pathways of Cr removal by Pd-biofilm and biofilm*

Pathways for the conversions of Cr mediated by Pd-biofilm and biofilm are depicted in Fig. 5. In Pd-biofilm (left side of Fig. 5), the predominant mechanisms was PdNP-catalyzed reduction of Cr(VI) to Cr (III), which led to the formation of $Cr(OH)_3$ precipitates, mostly on the surface of PdNPs (Eq. (3)):

$$1.5H_2 + CrO_4^{2-} + 2H^+ \xrightarrow{Pd} Cr(OH)_3\downarrow + H_2O \quad (3)$$

This mechanism shielded the bacteria from the toxic effects of Cr(VI) and enabled the removal of Cr through precipitation and immobilization as $Cr(OH)_3$. It also means that strictly microbial reduction of Cr(VI) played only a minor role.

For the non-Pd biofilm, bioreduction of Cr(VI) occurred via intracellular and extracellular pathways. Intracellular enzymes (e.g., YieF)

utilized NADPH (from H_2 oxidation) to reduce Cr(VI). Intracellular reduction involves cellular metabolites, e.g. cysteine and glutathione, which can form organo-Cr(III) complexes and would be released into the extracellular space (Joutey et al., 2015). Membrane reductases, including cytochromes, reduce Cr(VI) as an electron acceptor, producing Cr(III), which then complexed to functional groups in EPS. These complexation mechanisms, which are part of bacterial resistance of Cr (VI), accounted for the higher concentration of dissolved Cr(III) in the non-Pd MBfR effluent compared to the Pd-MBfR.

4. Conclusion

In-situ generated PdNPs associated with the biofilm led to more-rapid and -complete Cr(VI) reduction to Cr(III) and removal of TCr as $Cr(OH)_3$ solids in the Pd-MBfR system. A surface loading of 80 mg Cr m^{-2} d^{-1} consistently achieved 99 % reduction of Cr(VI) and removal of TCr to below 50 μg L^{-1} with the Pd-MBfR. In contrast, the non-Pd MBfR effluent contained 280–300 μg L^{-1} of dissolved Cr(III), which was present as soluble organo-Cr(III) complexes. Because the PdNPs protected the bacteria from the toxic effects of Cr, they minimized the release of soluble organics that formed the soluble organo-Cr(III) complexes that inhibited the precipitation of $Cr(OH)_3$ in the non-Pd MBfR. High-throughput sequencing and functional-gene prediction revealed a stable Pd-biofilm structure in the Pd-MBfR after Cr(VI) exposure, with the genus *Dechloromonas* dominating before and after Cr(VI) input. In the non-Pd MBfR, the introduction of Cr(VI) led to an increase in Cr(VI) reducers (*Sediminibacterium* and *Meiothermus*) and an upsurge in the abundance of genes related to chromate reduction and cellular metabolites involved in the formation of organo-Cr(III) complexes; these changes did not occur in the Pd-MBfR due to the protective nature of the PdNPs. This study demonstrates the promise of utilizing *in-situ* generated PdNPs immobilized on the biofilm for efficient removal of Cr from wastewater, and it provides mechanistic insights how the PdNPs protect the biofilm from toxicity and lead to more complete TCr removal.

Declaration of Competing Interest

The authors declare that they have no known competing financial interests or personal relationships that could have appeared to influence the work reported in this paper.

Data availability

Data will be made available on request.

Acknowledgements

The authors would like to acknowledge the co-funding of this work by the National Natural Science Foundation of China (No.52070130) and the Natural Science Foundation of Shanghai (No.22ZR1443200).

Supplementary materials

Supplementary material associated with this article can be found, in the online version, at doi:10.1016/j.watres.2023.120878.

References

Akob, D.M., Mills, H.J., Gihring, T.M., Kerkhof, L., Stucki, J.W., Anastácio, A.S., Chin, K. J., Küsel, K., Palumbo, A.V., Watson, D.B., Kostka, J.E., 2008. Functional diversity and electron donor dependence of microbial populations capable of U(VI) reduction in radionuclide-contaminated subsurface sediments. Appl. Environ. Microbiol. 74 (10), 3159–3170.

Bahafid, W., Sayel, H., Tahri Joutey, N., El Ghachtouli, N., 2011. Removal mechanism of hexavalent chromium by a novel strain of pichia anomala isolated from industrial effluents of fez (Morocco). J. Environ. Sci. Eng. 5, 980–991.

Caporaso, J.G., Kuczynski, J., Stombaugh, J., Bittinger, K., Bushman, F.D., Costello, E.K., Fierer, N., Peña, A.G., Goodrich, J.K., Gordon, J.I., Huttley, G.A., Kelley, S.T., Knights, D., Koenig, J.E., Ley, R.E., Lozupone, C.A., McDonald, D., Muegge, B.D., Pirrung, M., Reeder, J., Sevinsky, J.R., Turnbaugh, P.J., Walters, W.A., Widmann, J., Yatsunenko, T., Zaneveld, J., Knight, R., 2010. QIIME allows analysis of high-throughput community sequencing data. Nat. Methods 7 (5), 335–336.

Celebi, M., Yurderi, M., Bulut, A., Kaya, M., Zahmakiran, M., 2016. Palladium nanoparticles supported on amine-functionalized SiO_2 for the catalytic hexavalent chromium reduction. Appl. Catal. B Environ. 180, 53–64.

Cettn, Z., Kantar, C., Alpaslan, M., 2009. Interactions between uronic acids and chromium(III). Environ. Toxicol. Chem. 28 (8), 1599–1608.

Chi, Z., Ju, S., Wang, W., Li, H., Luo, Y., Rittmann, B.E., 2023. Ethane-driven chromate and nitrate bioreductions in a membrane biofilm reactor. Chem. Eng. J. 452, 139135.

Coby, A.J., Picardal, F., Shelobolina, E., Xu, H., Roden, E.E., 2011. Repeated anaerobic microbial redox cycling of iron. Appl. Environ. Microbiol. 77 (17), 6036–6042.

Dogan, N.M., Kantar, C., Gulcan, S., Dodge, C.J., Yilmaz, B.C., Mazmanci, M.A., 2011. Chromium(VI) bioremoval by pseudomonas bacteria: role of microbial exudates for natural attenuation and biotreatment of Cr(VI) contamination. Environ. Sci. Technol. 45 (6), 2278–2285.

Frølund, B., Palmgren, R., Keiding, K., Nielsen, P.H., 1996. Extraction of extracellular polymers from activated sludge using a cation exchange resin. Water Res. 30 (8), 1749–1758.

Guo, S., Heck, K., Kasiraju, S., Qian, H., Zhao, Z., Grabow, L.C., Miller, J.T., Wong, M.S., 2018. Insights into nitrate reduction over indium-decorated palladium nanoparticle catalysts. ACS Catal. 8 (1), 503–515.

Jobby, R., Jha, P., Yadav, A.K., Desai, N., 2018. Biosorption and biotransformation of hexavalent chromium [Cr(VI)]: a comprehensive review. Chemosphere 207, 255–266.

Joutey, N.T., Sayel, H., Bahafid, W., El Ghachtouli, N., 2015. Mechanisms of hexavalent chromium resistance and removal by microorganisms. Rev. Environ. Contam. Toxicol. 233, 45–69.

Kantar, C., Cetin, Z., Demiray, H., 2008. *In situ* stabilization of chromium(VI) in polluted soils using organic ligands: the role of galacturonic, glucuronic and alginic acids. J. Hazard. Mater. 159 (2), 287–293.

Lai, C., Zhong, L., Zhang, Y., Chen, J., Wen, L., Shi, L.D., Sun, Y, Ma, F., Rittmann, B.E., Zhou, C., Tang, Y., Zheng, P., Zhao, H., 2016. Bioreduction of chromate in a methane-based membrane biofilm reactor. Environ. Sci. Technol. 50 (11), 5832–5839.

Langille, M.G.I., Zaneveld, J., Caporaso, J.G., McDonald, D., Knights, D., Reyes, J.A., Clemente, J.C., Burkepile, D.E., Vega Thurber, R.L., Knight, R., Beiko, R.G., Huttenhower, C., 2013. Predictive functional profiling of microbial communities using 16S rRNA marker gene sequences. Nat. Biotechnol. 31 (9), 814–821.

Long, M., Long, X., Zheng, C., Luo, Y., Zhou, C., Rittmann, B.E., 2021. Para-chlorophenol (4-CP) removal by a palladium-coated biofilm: coupling catalytic dechlorination and microbial mineralization via denitrification. Environ. Sci. Technol. 55 (9), 6309–6319.

Long, M., Zhou, C., Xia, S., Guadiea, A., 2017. Concomitant Cr(VI) reduction and Cr(III) precipitation with nitrate in a methane/oxygen-based membrane biofilm reactor. Chem. Eng. J. 315, 58–66.

Luo, X., Zhou, X., Peng, C., Shao, P., Wei, F., Li, S., Liu, T., Yang, L., Ding, L., Luo, X., 2022. Bioreduction performance of Cr(VI) by microbial extracellular polymeric substances (EPS) and the overlooked role of tryptophan. J. Hazard. Mater. 433, 128822.

Munoz, M., Kolb, V., Lamolda, A., de Pedro, Z.M., Modrow, A., Etzold, B.J.M., Rodriguez, J.J., Casas, J.A., 2017. Polymer-based spherical activated carbon as catalytic support for hydrodechlorination reactions. Appl. Catal. B Environ. 218, 498–505.

Pierce, J., Suelter, C.H., 1977. An evaluation of the Coomassie brilliant blue G-250 dye-binding method for quantitative protein determination. Anal. Biochem. 81 (2), 478–480.

Pradhan, D., Sukla, L.B., Sawyer, M., Rahman, P.K.S.M., 2017. Recent bioreduction of hexavalent chromium in wastewater treatment: a review. J. Ind. Eng. Chem. 55, 1–20.

Puzon, G.J., Roberts, A.G., Kramer, D.M., Xun, L., 2005. Formation of soluble organo-chromium(III) complexes after chromate reduction in the presence of cellular organics. Environ. Sci. Technol. 39 (8), 2811–2817.

Rittmann, B.E., McCarty, P.L., 2020. Environmental Biotechnology: Principles and Applications. McGraw-Hill Book Co., New York.

Ramírez-Díaz, M.I., Díaz-Pérez, C., Vargas, E., Riveros-Rosas, H., Campos-García, J., Cervantes, C., 2008. Mechanisms of bacterial resistance to chromium compounds. BioMetals 21 (3), 321–332.

Tang, Y., Zhou, C., Van Ginkel, S.W., Ontiveros-Valencia, A., Shin, J., Rittmann, B.E., 2012. Hydrogen permeability of the hollow fibers used in H_2-based membrane biofilm reactors. J. Membr. Sci. 407 (408), 176–183.

Thatoi, H., Das, S., Mishra, J., Rath, B.P., Das, N., 2014. Bacterial chromate reductase, a potential enzyme for bioremediation of hexavalent chromium: a review. J. Environ. Manag. 146, 383–399.

United States Environmental Protection Agency. 2015. Appendix A to Subpart O-Regulated Contaminants.

Wu, C., Zhou, L., Zhou, C., Zhou, Y., Xia, S., Rittmann, B.E., 2022a. Co-removal of 2,4-dichlorophenol and nitrate using a palladized biofilm: denitrification-promoted microbial mineralization following catalytic dechlorination. J. Hazard. Mater. 422, 126916.

Wu, C., Zhou, L., Zhou, C., Zhou, Y., Zhou, J., Xia, S., Rittmann, B.E., 2022b. A kinetic model for 2,4-dichlorophenol adsorption and hydrodechlorination over a palladized biofilm. Water Res. 214, 118201.

Wu, C., Zhou, L., Zhou, Y., Zhou, C., Xia, S., Rittmann, B.E., 2021. Dechlorination of 2,4-dichlorophenol in a hydrogen-based membrane palladium-film reactor: performance, mechanisms, and model development. Water Res. 188, 116465.

Xi, Y., Zhang, Y., Cai, X., Fan, Z., Wang, K., Dong, W., Shen, Y., Zhong, S., Yang, L., Bai, S., 2022. PtCu thickness-modulated interfacial charge transfer and surface reactivity in stacked graphene/Pd@PtCu heterostructures for highly efficient visible-light reduction of CO_2 to CH_4. Appl. Catal. B Environ. 305, 121069.

Xia, S., Xu, X., Zhou, C., Wang, C., Zhou, L., Rittmann, B.E., 2016. Direct delivery of CO_2 into a hydrogen-based membrane biofilm reactor and model development. Chem. Eng. J. 290, 154–160.

Xie, W., Wang, F., Guo, L., Chen, Z., Sievert, S.M., Meng, J., Huang, G., Li, Y., Yan, Q., Wu, S., Wang, X., Chen, S., He, G., Xiao, X., Xu, A., 2011. Comparative metagenomics of microbial communities inhabiting deep-sea hydrothermal vent chimneys with contrasting chemistries. ISME J. 5 (3), 414–426.

Yin, Y.B., Guo, S., Heck, K.N., Clark, C.A., Conrad, C.L., Wong, M.S., 2018. Treating water by degrading oxyanions using metallic nanostructures. ACS Sustain. Chem. Eng. 6 (9), 11160–11175.

Zhao, Y., Wang, Q., Yang, Z., Jia, X., Cabrera, J., Ji, M., 2022. Bio-capture of Cr(VI) in a denitrification system: electron competition, long-term performance, and microbial community evolution. J. Hazard. Mater. 432, 128697.

Zhou, C., Ontiveros-Valencia, A., Nerenberg, R., Tang, Y., Friese, D., Krajmalnik-Brown, R., Rittmann, B.E., 2019. Hydrogenotrophic microbial reduction of oxyanions with the membrane biofilm reactor. Front. Microbiol. 9, 3268.

Zhou, C., Ontiveros-Valencia, A., Wang, Z., Maldonado, J., Zhao, H., Krajmalnik-Brown, R., Rittmann, B.E., 2016. Palladium recovery in a H_2-based membrane biofilm reactor: formation of Pd(0) nanoparticles through enzymatic and autocatalytic reductions. Environ. Sci. Technol. 50 (5), 2546–2555.

Zhou, D., Luo, Y., Zheng, C., Long, M., Long, X., Bi, Y., Zheng, X., Zhou, C., Rittmann, B. E., 2021. H_2-based membrane catalyst-film reactor (H_2-MCfR) loaded with palladium for removing oxidized contaminants in water. Environ. Sci. Technol. 55 (10), 7082–7093.

Supplementary material

Reduction and precipitation of chromium(VI) using a palladized membrane biofilm reactor

Chengyang Wu [a, §], Jingzhou Zhou [b, §], Si Pang [b], Lin Yang [b], Eric Lichtfouse [c], Hongbo Liu [a,*], Siqing Xia [b], Bruce E. Rittmann [c]

[a] *School of Environment and Architecture, University of Shanghai for Science and Technology, 516 Jungong Road, Shanghai, China*

[b] *State Key Laboratory of Pollution Control and Resource Reuse, College of Environmental Science and Engineering, Tongji University, 1239 Siping Road, Shanghai, China*

[c] *Aix-Marseille Univ, CNRS, IRD, INRA, Coll France, CEREGE, 13100 Aix en Provence, France*

[d] *Biodesign Swette Center for Environmental Biotechnology, Arizona State University, 727 Tyler Road, Tempe, USA*

§ Chengyang Wu and Jingzhou Zhou equally contributed to this work.

* Corresponding author

E-mail address: Liuhb@usst.edu.cn (H. Liu)

Summary:

Pages: 7

Figures: 5

Tables: 3

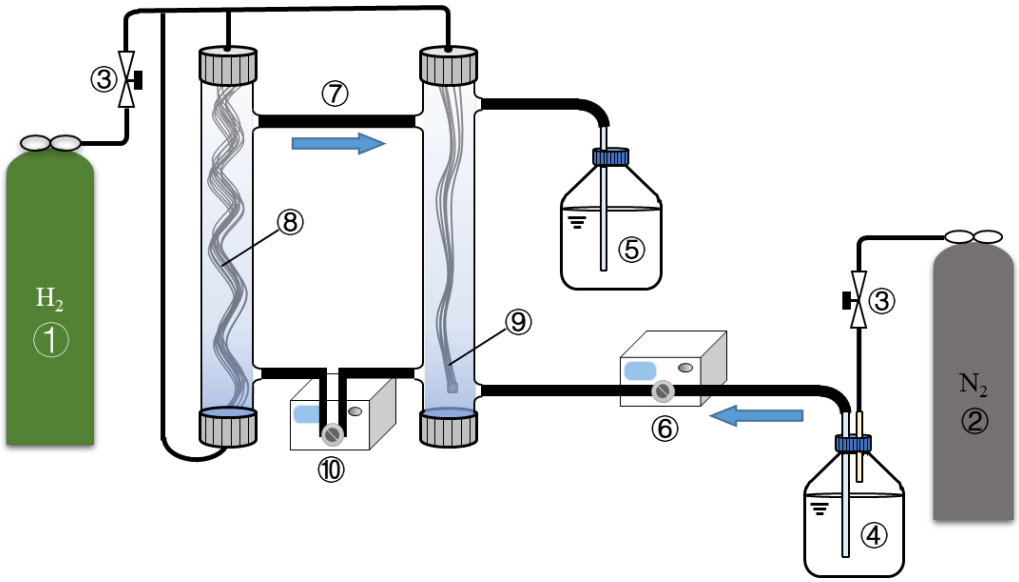

Figure S1. Schematic of the Pd-MBfR system: ① pure-H_2 gas tank to feed the fiber bundles; ② pure-N_2 gas to feed the headspace of the influent medium bottle; ③ gas-pressure regulator; ④ influent-medium bottle; ⑤ effluent bottle; ⑥ influent pump; ⑦ Recirculation configuration (the blue arrow indicates the flow direction); ⑧ main bundle with 32 fibers; ⑨ sampling coupon bundle with 10 fibers; and ⑩ recirculation pump.

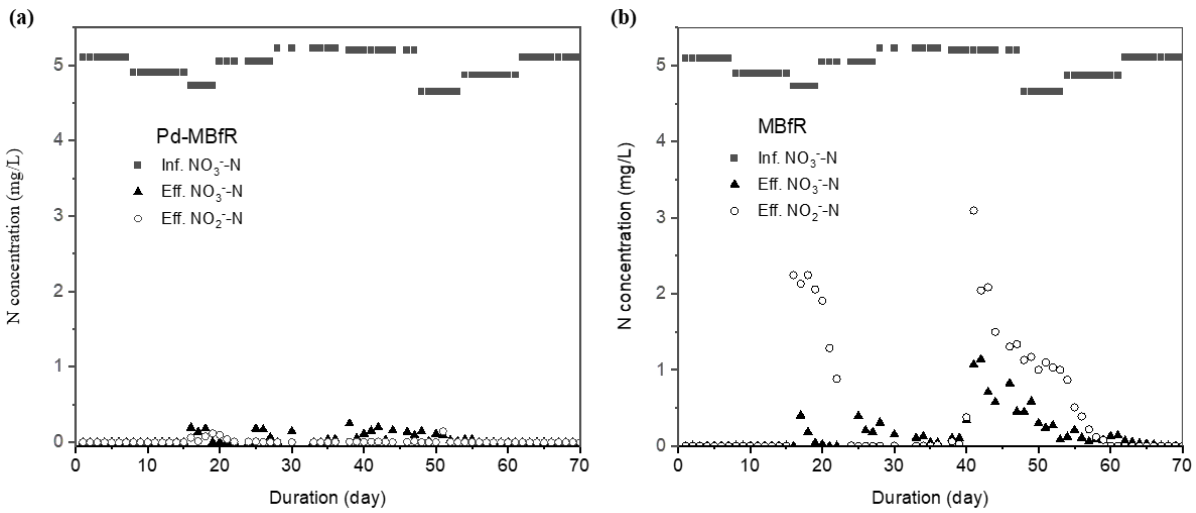

Figure S2. NO_3^- and NO_2^- concentrations (mg N/L) in the influent and the effluent of the Pd-MBfR (a) and MBfR (b).

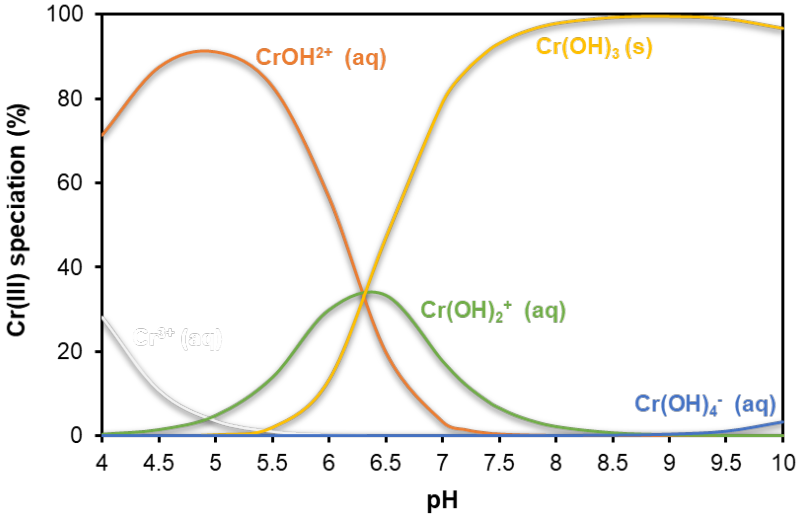

Figure S3. Cr(III) speciation as a function of pH computed by Visual MINTEQ, with the default values $[Cr(III)]_{total}$ = 1 mg L^{-1}, ionic strength calculated, temperature (T) = 25°C, and the only Cr(III) species being Cr^{3+} and its complexes with HO^-.

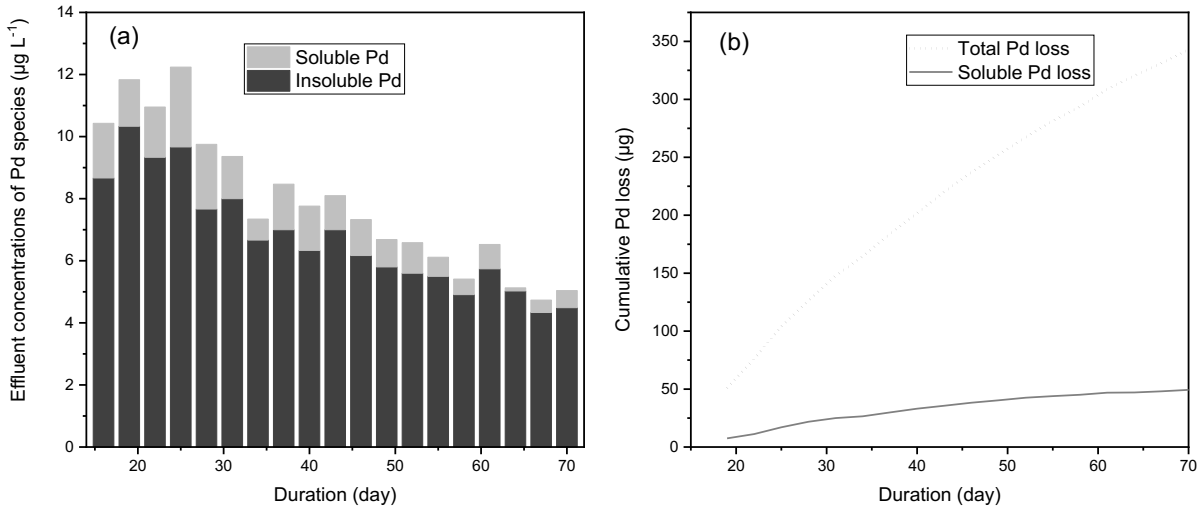

Figure S4. The effluent concentrations of total Pd, soluble Pd(II), and insoluble Pd(0) (a), as well as cumulative Pd loss during continuous operation (b). The concentration of insoluble Pd was calculated by subtracting soluble Pd from total Pd in the effluent.

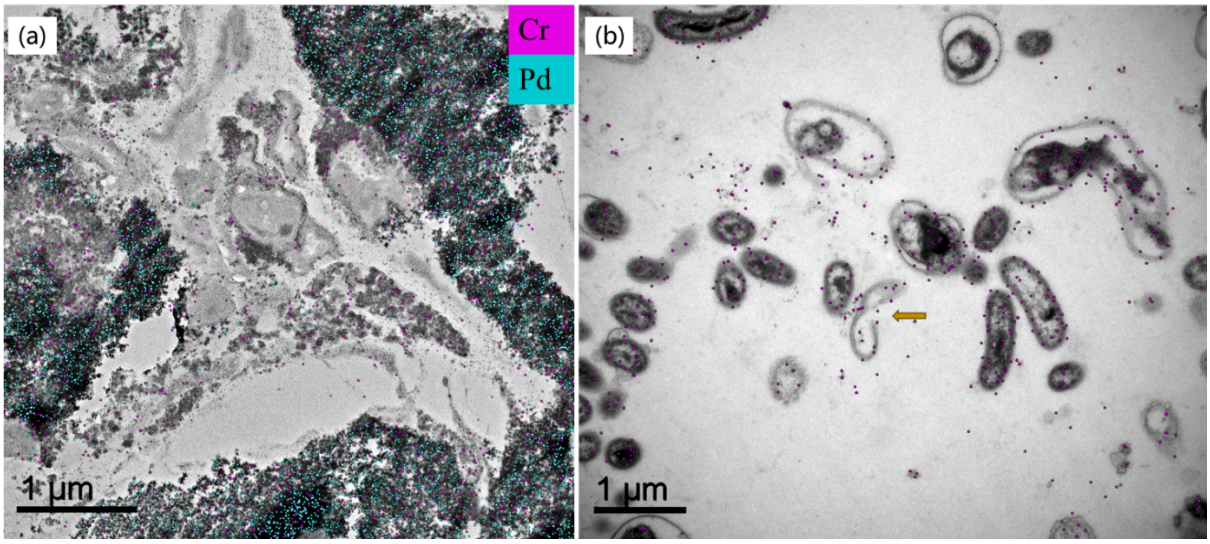

Figure S5. TEM images of the biofilm cells and precipitates immobilized in Pd-biofilm (a) and biofilm (b). The grey shapes are bacterial cells, and the dark spots are Pd or Cr (confirmed by EDX signals).

Process of raw sequences in microbial community analyses

We removed sequences shorter than 200 bps, homopolymers of more than 6 bps, and primer mismatches, or a quality score lower than 25. Chimeric sequences were removed by HCHIME and then the operational taxonomic unit (OTUs) was clustered with 97% similarity cutoff using UPARSE (version 7.0.1). Representative sequences were aligned to the silva (SSU138) 16S rRNA database by RDP Classifier (version 2.11), using confidence threshold of 0.7.

Table S1. Composition of the mineral-salts medium fed to the reactors

Component	Concentration ($mg \cdot L^{-1}$)	Contents	Concentration ($mg \cdot L^{-1}$)
$NaHCO_3$	50	$ZnCl_2$	0.070
KH_2PO_4	20	$Na_2MoO_4 \cdot 2H_2O$	0.036
$MgCl_2 \cdot 6H_2O$	2.0	$NiCl_2 \cdot 6H_2O$	0.024
$FeCl_2 \cdot 4H_2O$	0.10	Na_2SeO_3	0.009
$CaCl_2 \cdot 2H_2O$	0.10	$Na_2WO_4 \cdot 2H_2O$	0.008
$CoCl_2 \cdot 6H_2O$	0.19	H_3BO_3	0.006
$MnCl_2 \cdot 4H_2O$	0.10	$CuCl_2 \cdot 2H_2O$	0.002

Table S2. The excitation/emission wavelength and the responded components of the five Regions in the EEM spectra.

Region	Ex/Em (nm)	Components
I	200-250/280-330	Aromatic protein I
II	200-250/330-380	Aromatic protein II
III	200-250/380-550	Fulvic acid-like matters
IV	>250/280-380	Protein-like substances
V	>250/380-550	Humic acid-like matters

Table S3. Parameter settings of the 3D fluorescence spectrometer.

Parameters	Set values
Excitation wavelength range	220.0~400.0 nm
Emission wavelength range	260.0~550.0 nm
Excited broadband	2.0 nm
Launch broadband	2.0 nm
Scan rate	1200 nm/min
Excitation unit slit width	2.5 nm
Slot width of transmitting unit	2.5 nm
Photocell voltage	700V

References Cited in the SI

[1] Xia, S., Xu, X., Zhou, C., Wang, C., Zhou, L., Rittmann, B.E., Direct delivery of CO_2 into a hydrogen-based membrane biofilm reactor and model development, Chemical Engineering Journal 290 (2016), 154-160.

[2] Zhou C, Ontiveros-Valencia A, Wang Z, Maldonado J, Zhao H-P, Krajmalnik-Brown R, Rittmann B E. Palladium recovery in a H_2-based membrane biofilm reactor: Formation of Pd(0) nanoparticles through enzymatic and autocatalytic reductions. Environmental Science & Technology 50(5) (2016), 2546-2555.

[3] Zhou, Y., Li, R., Guo, B., Xia, S., Liu, Y., Rittmann, B.E., The influent COD/N ratio controlled the linear alkylbenzene sulfonate biodegradation and extracellular polymeric substances accumulation in an oxygen-based membrane biofilm reactor. Journal of Hazardous Materials 422 (2022), 126862.